

Supplementary Information

Liquid metal nanodroplet dynamics inside nanocontainers

Hyun Young Jung¹, Hyunkyung Chun¹, Sora Park², Seoung-Hun Kang², Chi Won Ahn³, Young-Kyun Kwon², Moneesh Upmanyu¹, Pulickel M. Ajayan^{4*}, & Yung Joon Jung^{1,2*}

¹Department of Mechanical and Industrial Engineering, Northeastern University, Boston, Massachusetts, 02115, USA,

²Department of Physics and Research Institute for Basic Sciences, Kyung Hee University, Seoul, 130-701, Korea.

³Nano-Materials Lab, National NanoFab Center, Korea Advanced Institute of Science and Technology, 53-3 Eoeun-dong, Yuseong-gu, Daejeon, 305-806, Republic of Korea.

⁴Department of Mechanical Engineering and Material Science, Rice University, Houston, Texas, 77005, USA.

Supplementary Text

Temperature dependence of total energy and specific heat per atom: To investigate the melting point of the lead nanodroplets, we performed molecular dynamics simulations based on *ab initio* calculations within the framework of the density functional theory (DFT). Figure S1a-1b show the temperature dependence of the total energy $E(T)$ of the Pb bulk structure and Pb₅₅ nanoparticle, which clearly displays their phase transition temperatures. The $E(T)$ curves for both the bulk and the nanoparticle increase steadily with increasing temperature. The noticeable feature in the graph is a well-formed step at $T=900$ K and $T=680$ K indicating the “phase transition,” or melting of the respective systems. To verify the size effect in the melting temperature, we also did for Pb₁₃ nanoparticle, which exhibits much broad step around $T=500$ K (not shown in the figure). We also calculated the temperature dependence of the specific heat per atom $C_v(T)$ obtained from $C_v(T) = dE/dT$, shown in Fig. S1c-1d for respective cases. In the temperature range addressed in this study, we found the calculated values are close to the classical value $C_v=3k_B$, where k_B is the Boltzmann

constant. Individual peaks in the specific heat reflect the latent heat of transition between different phases.

From the maximum value of specific heat $C_v(T)$ one can obtain the melting point, and from the height of the smoothed-out step in the caloric curve one gets the latent heat of fusion q , that is, the energy necessary to destroy the crystalline lattice at the melting point. An abrupt jump in the internal enthalpy observed during heating the bulk system does not reflect the true thermodynamic melting because periodic boundary condition used in calculations provides no heterogeneous nucleation site, such as free surface or the solid-liquid interface. Another reason is that the DFT is known to provide overbinding in the cohesive energy (see the methods section). Thus the calculated melting temperatures are higher than the true melting temperatures observed experimentally. To estimate the true melting temperature of nanoparticles, we considered the ratio $R = 680/900$ of the melting temperature of nanoparticle to the bulk melting temperature obtained in our MD simulations and the true melting temperature of the bulk, i.e., $T_{mp} = RT_{mb}$. This fact reveals that the confined nanoparticle can be significantly superheated at about 460 K compare with experimental T_{mb} of 601 K.

Dynamics of partially wetted metal nanodroplets: The in-situ characterization reveals changes in morphology of the nanodroplets during their dynamic evolution. Since each nanodroplet-nanocup system is effectively a closed thermodynamic system, the morphological evolution is a reflection of the combined effect of evaporation-condensation at the droplet surfaces as well as their interactions with the nanocup walls. In order to illustrate how these effects shape the dynamics of the droplets, consider a single droplet composed of n_d Pb atoms inside a sealed nanocup (Fig. S3). The equilibrium droplet shape satisfies the Young's balance at the enveloping contact line, $\cos \theta = \Gamma$, where θ is the equilibrium contact angle and Γ is the ratio of the energy of the droplet-nanocup interface to that of the droplet-vapor interface, $\Gamma = \gamma_{lc}/\gamma_{lv}$.

The contact angle, the droplet shape and the equilibrium Pb vapor pressure within the nanocup together set its size. In addition, at the ambient temperature T the droplet must provide and also be in

equilibrium with its vapor. To capture the effect of this interplay on the equilibrium droplet size, we approximate the shape as a spherical cap of radius R . The radius sets the droplet volume V_d and therefore the number of atoms n_d , i.e.

$$V_d = \left[\frac{3\Gamma}{\pi\{4\Gamma - (1-\Gamma^2)^2\}} \right] R^3 = f(\Gamma)R^3, \text{ and} \quad (\text{S1})$$

$$n_d = \frac{N_A}{M_{Pb}\rho_{Pb}} V_d = \alpha V_d,$$

where M_{Pb} and ρ_{Pb} are the atomic mass and density of lead, respectively, and N_A is Avogadro's number. We expect the atomic volume in the vapor phase to be much larger than that in the liquid phase, and the vapor can therefore be assumed to be an ideal gas. Then, the number of molecules in the vapor n_v is determined by the available volume,

$$n_v = \frac{p_{ve}(V_0 - V_d)}{k_B T}, \quad (\text{S2})$$

where V_0 is the volume of the nanocup and p_{ve} is the equilibrium vapor pressure. The latter is modified due to the large surface curvature of the nanoscopic droplets studied here (Kelvin effect), i.e.

$$p_{ve}(R) = p_{ve}(\infty) \exp\left(\frac{\Omega_v \gamma_{lv} 2}{k_B T R}\right) \equiv p_{ve}(\infty) \exp\left[\frac{\beta}{L R}\right], \quad (\text{S3})$$

where Ω_v is the atomic volume within the vapor phase. Finally, the entire system conserves its mass during the equilibration,

$$\delta n_d = -\delta n_v. \quad (\text{S4})$$

Combining Eqs. S2-S4,

$$\frac{\delta n_d}{\delta R} = \frac{p_{ve}(R)}{k_B T} \left[\frac{\delta V_d}{\delta R} + \frac{\beta}{R^2} (V_0 - V_d) \right], \quad (\text{S5})$$

and using Eq. S1 in S5, we get

$$\alpha f(\Gamma) R^2 = \frac{p_{ve}(R)}{k_B T} \left[\frac{\beta V_0}{3R^2} - \beta f(\Gamma) R + f(\Gamma) R^2 \right], \quad (\text{S6})$$

Equation S6 captures the interplay between geometry and thermodynamics that sets the droplet size R_{eq} and preserves the *local* Young's balance at the contact line. The final equilibrated system is

associated with net interface energy excess, defined here with respect to a suspended spherical droplet, takes the form

$$\Delta\gamma = \pi R^2[(1 - \Gamma^2)(\gamma_{lc} - \gamma_c) + 2(\Gamma - 1)\gamma_{lv}], \quad (1)$$

i.e. the excess interface energy scales as R^2 .

Driving force for active motions: Particles surrounded by ambient gas or liquid are constantly moving due to continuous collisions with the surrounding molecules. However, if surrounding molecules do not exist around a nanodroplet, what is the initial driving force for such active motions? For this experiment, there are two direct or indirect external sources that can affect the nanodroplet moving. First, in a TEM the nanodroplet is exposed to irradiation with electrons whose energy is given by the acceleration voltage of 300 kV. The maximum transferable kinetic energy, E_{\max} , to the nanodroplet from an incident electron can be estimated from the following equation¹: $E_{\max} = \frac{2E_k(E_k + 2mc^2)}{Mc^2}$, where in developing special relativity theory, the kinetic energy of a moving body is $E_k = mc^2(\gamma - 1)$; M and m are the mass of a nanodroplet and rest electron, and the Lorentz factor $\gamma = 1/\sqrt{1 - \frac{v^2}{c^2}}$; v and c are the speed of electron and light, respectively. The mass and speed are 4.46×10^{-20} Kg and 4.8×10^{-8} m/s (the mean velocity measured over an interval of time t is $\bar{v} \equiv \sqrt{4\sqrt{D}/\sqrt{t}}$) for the 20nm nanodroplet and 9.11×10^{-31} Kg and 2.33×10^8 m/s for the electron. The calculated maximum transferable energy is 5.12×10^{-24} J. The maximum momentum transferred to the nanodroplet, P , can be calculated as $P = \sqrt{2ME_{\max}}$ and for 20 nm nanodroplet, the value is 6.76×10^{-22} kg·m/s and is larger than the momentum of the nanodroplet measured experimentally. This means that the incident electrons have the potential to provide energy transfer to cause the random motions but not enough.

Important point to consider here is the total energy dissipation in the specimen. Hobbs has calculated the effects of beam current and thermal conductivity on the specimen temperature, as shown in ref. (2-3). A nanodroplet can often be considered as “zero-dimensional” objects, but they are held inside

a carbon container on a copper grid in the TEM. Heat dissipation occurs by heat conduction through the contact area and by thermal radiation. As a consequence, the overall heating of nanodroplets under the beam is typically a few degrees only. Therefore, thermal effects by the TEM beam can mostly be neglected when radiation-induced alterations in inorganic Pb nanodroplet are considered.

Second, external temperature has a marked effect. The molecules of matter at ordinary temperatures can be considered to be in ceaseless, random motion with a mean kinetic energy proportional to the temperature. The average translational kinetic energy for these molecules can be deduced from the Boltzmann distribution. The distribution function can be used to calculate the average value of the square of the velocity. The thermal energy of the nanodroplet consisting of N atoms is given by the sum of these energies, assuming no losses to the container or the environment: $U_{\text{thermal}} = \frac{1}{2}Nmv^2 = \frac{3}{2}NkT$. For 20 nm nanodroplet the thermal energy at 600 K is calculated as 1.6×10^{-15} J. This value is much higher than the energy transferred by the TEM beam. Although transferable energy of incident electrons in TEM can contribute particle motion, the shape of initial nanoparticles at 300 K was not changed by TEM electrons (shown in the supplemental Fig. S4 and movie S4), which indicates incident electrons may not transfer a sufficient momentum to cause this random motion. Also the large deformations of the lead droplet can be considered by changes in the interfacial free energy of the drop, which such energy differences are order $\sigma(\pi R^2)$ where $\sigma \sim 400$ mJ/m² is the surface tension of molten lead and $R \sim 10$ nm is the radius of the droplet. However, this interfacial energy (1.6×10^{-16} J) is much smaller than the thermal energy. Therefore, we believe that external temperature has the most marked effect.

As particle downsizing continues, the specific surface area increases generally in reversal proportion to the particle size. Due to the open surface it is generally easier to displace a surface atom than an atom inside the bulk. For the Pb nanodroplet with 20 nm in diameter, the number of atoms at the surface in total number of about 4.4×10^4 atoms is about 2700 corresponding that the fraction of

surface atoms is 6%, while that of a single larger nanodroplet with 50 nm diameter (shown in Fig. 1c, 1f and Fig. 2a) is only 1.8%. Therefore, cluster evaporation or displacement from nanodroplets could be activated more effectively due to the weakly bonded Pb atoms in the surface.

In the case of electron-induced atomic displacements, minimum threshold incident electron energy (E_t^{\min}) to displace atoms from the surface is found by solving the following equation⁴: $E_t^{\min} = (511 \text{ keV})\{[1 + AE_d/(561 \text{ eV})^{1/2} - 1]\}$, where A is the atomic mass number and E_d is the displacement energy. For Pb metal, E_d is 19 eV⁵ and as a result the threshold energy needs 840 keV. Therefore, no atom displacements are possible at applied threshold energy of 300 keV electron beam, whereas the external thermal energy can create detached clusters from the surface of nanodroplet because it can provide enough energy to release the surface atoms of Pb with surface binding energy of 2.5 eV⁶. In actuality, by heating under low pressure more and more clusters are detached from the nanodroplets and are energetically excited. Once more surface atoms in nanoparticles are energetically excited, more atomistic clusters can be relaxed from Pb nanoparticles. Therefore, the observed irregular motions of nanodroplets are due to the transfer of energy and momentum and molecular collisions from the clusters generated by the external heating onto the nanodroplets.

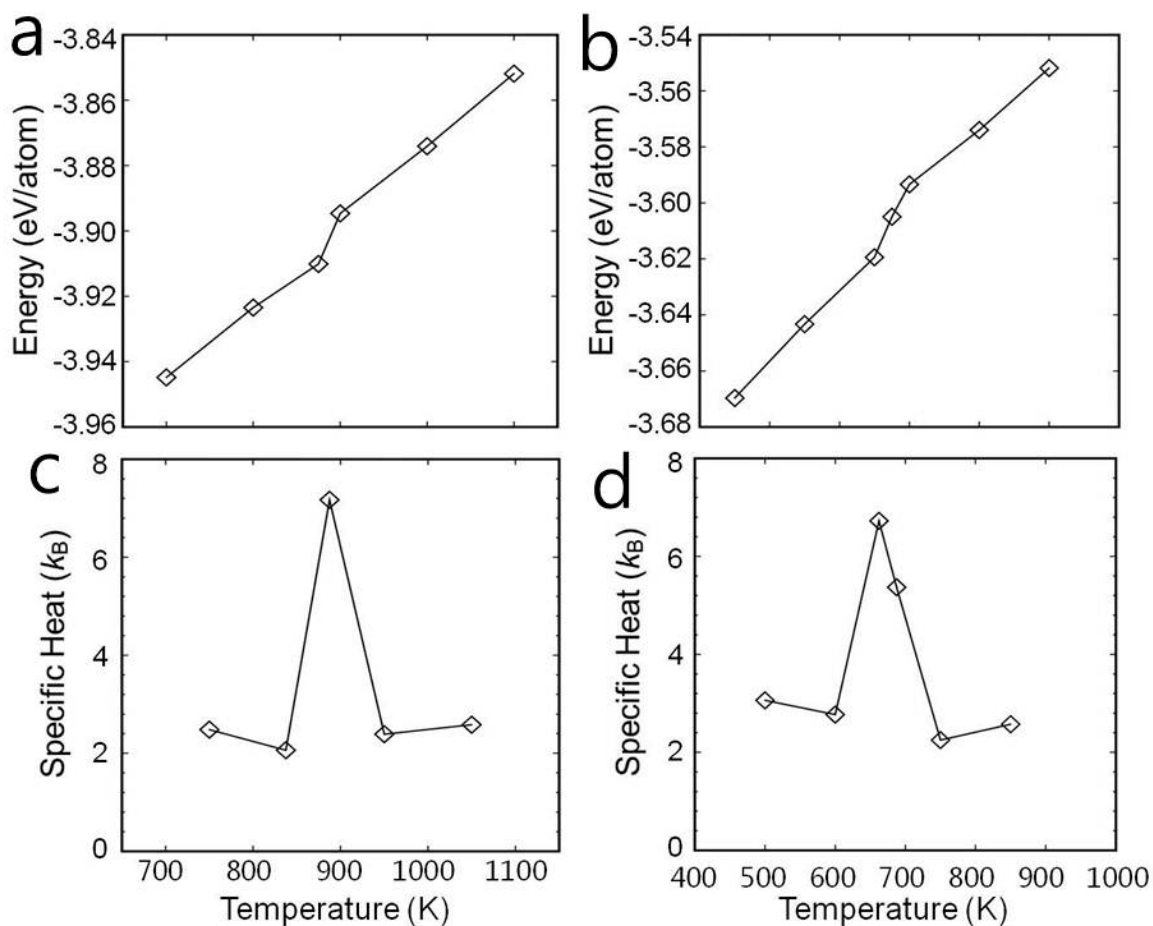


Figure S1 | Temperature dependence of total energy and specific heat per atom. Temperature dependence of the total energy E (a and b) and specific heat C_v (c and d) per atom for (a and c) the bulk of Pb and (b and d) Pb_{55} nanocluster. The data points in the $E(T)$ curve for the bulk of Pb and Pb_{55} nanocluster mark the discrete steps of the heat bath temperature range from 700 K to 1100 K.

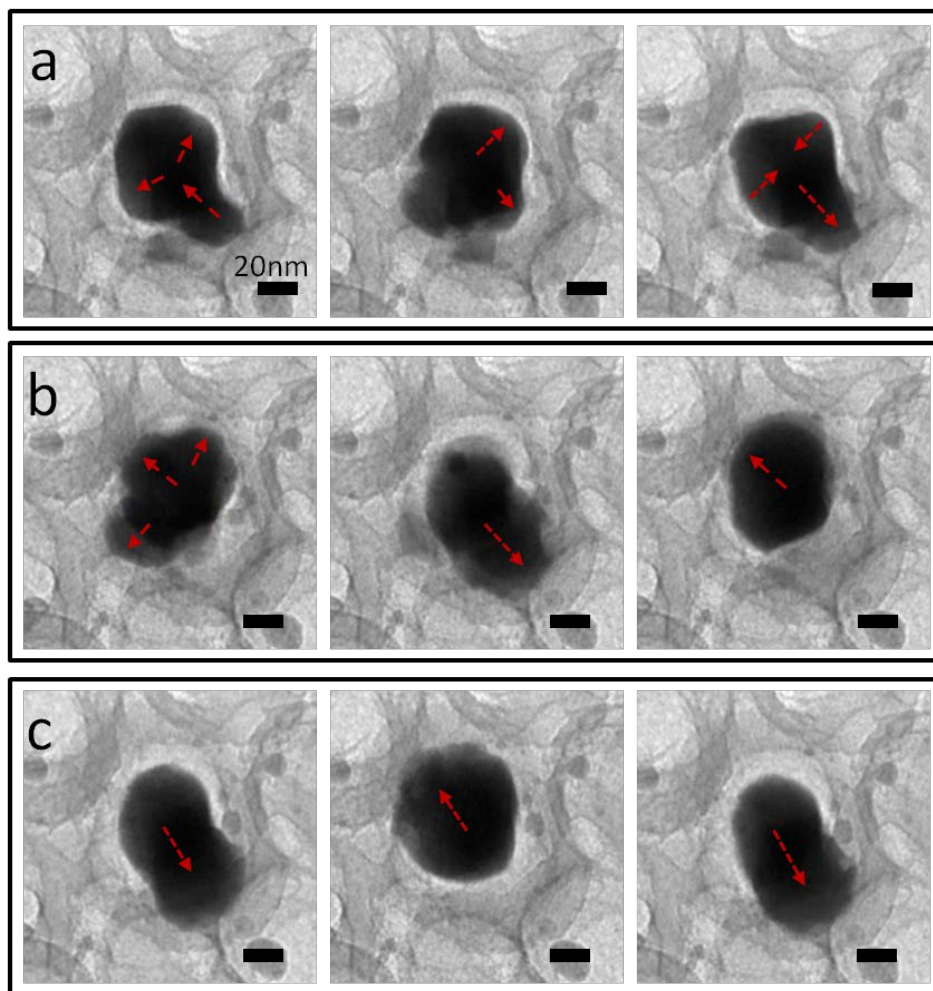


Figure S2 | The dynamic motion of a large Pb nanoparticle as function of time inside closed nanocup at 630 K. TEM images were taken after tilting TEM holder by 30° in x-axis. The image sequence shows dynamic motion of large size Pb at 630 K inside nanocup system which is geometrically completely closed in nanoscale and red dotted arrows indicate the direction of its motion. (a) Images at 6.83s, 7.07s and 7.83s respectively. The nanoparticle in early stage at 630 K shows active movement in random directions and the shape of Pb is irregular. As time increases, the major motion occurs along with the axial direction of the structure and the shape of Pb changes to more round shape (b and c). (b) Images at 25.27s, 25.63s and 25.90s respectively. (c) Images at 44.43s, 45.13s and 46.00s respectively. Scale bars are 20nm.

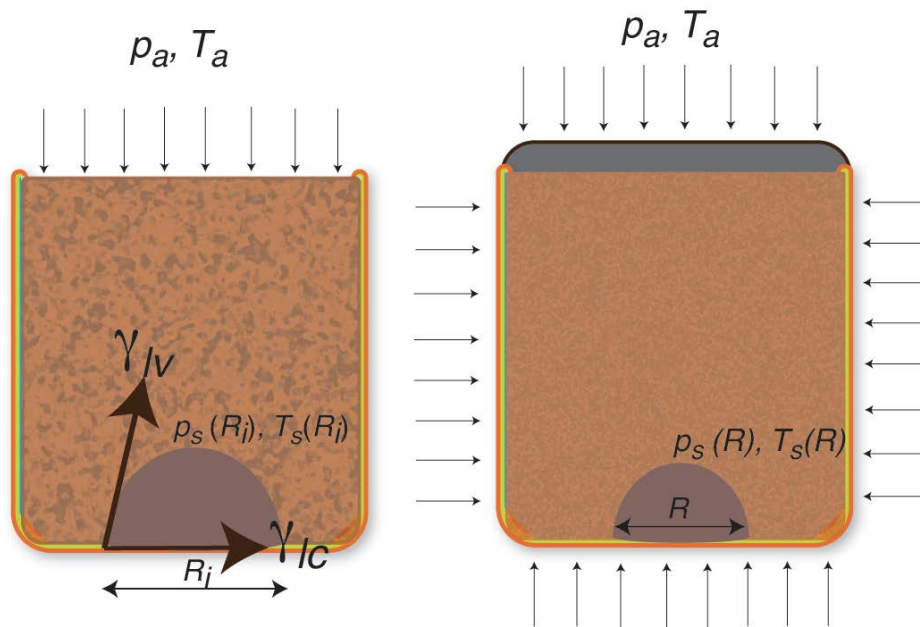


Figure S3 | Dynamics of partially wetted metal nanodroplets. The in-situ characterization reveals changes in morphology of the nanodroplets during their dynamic evolution.

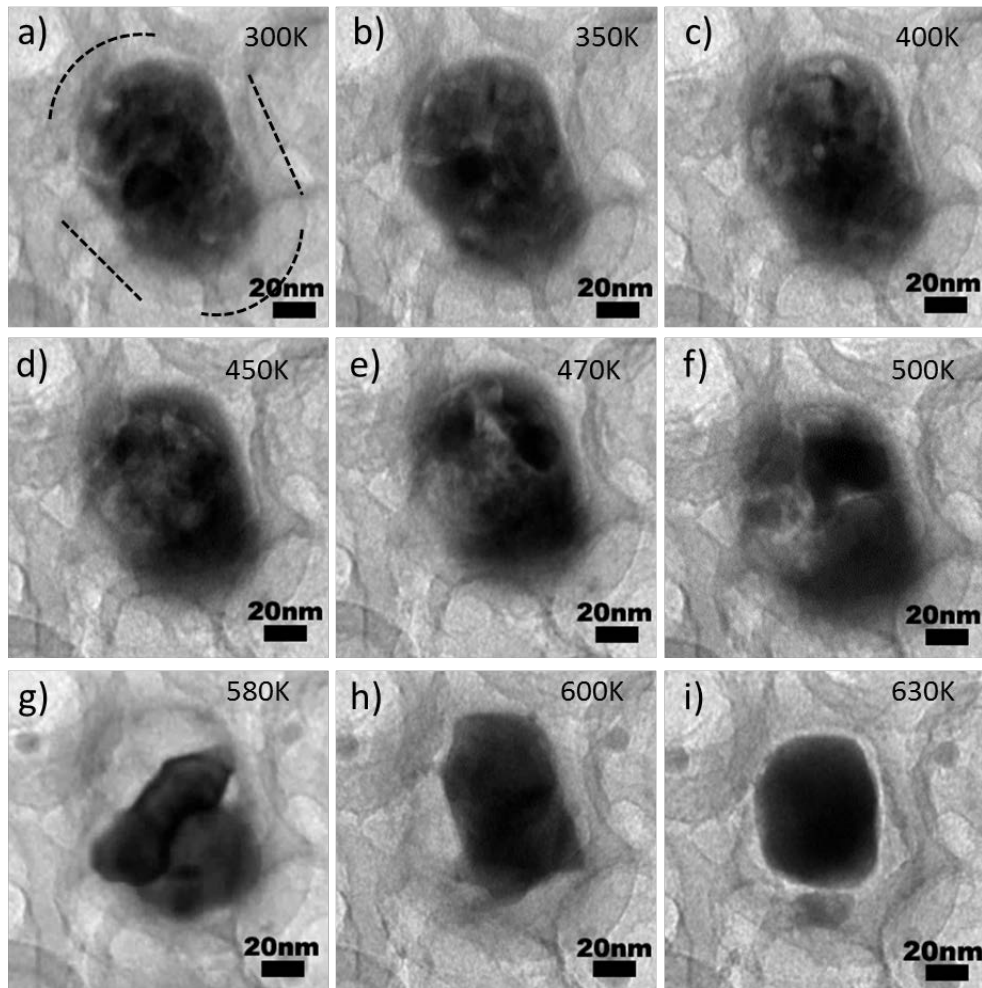


Figure S4 | TEM images of phase transition of a large Pb particle in the closed nanocup system while increasing temperature. Phase transition of a Pb nanoparticle inside a nanocup at different temperature. In situ electron microscopy studies were undertaken in a JEOL-3011 (HR) with an accelerating voltage of 300kV equipped with a heating specimen stage. Double tilt heating holder was used for placing sample and it was tilted by 30° in x-axis during imaging. Video images were taken by Gatan CCD camera with frame rate of 30. When the temperature started to increase from room temperature, localized nucleation on the Pb surface started slowly. At around 470 K, the single large solid Pb nanoparticle was liquidified and clusters were detached from the surface of liquid Pb nanoparticle and were released into the empty space inside nanocup. The presence of clusters in empty space resulted into a pressurized system inside nanocup. At 600 K, it takes shape in a body because their thermal activation energy is used to change of state. At 630 K, the liquid Pb nanoparticle moves ceaselessly and rapidly in the carbon reactor until their shape is rounded.

Movie S1 | Motion of a melted large Pb nanoparticle. A melted large Pb nanoparticle starts to fluctuate in both axial and radial directions inside the cylindrical nanocup. With time, this motion becomes more along the axial direction of the nanocontainer following the cylindrical empty space that exists in the nanocup container.

Movie S2 | Smaller droplets ceaselessly moved inside the nanocontainer. Individual movement of each nanodroplet appeared random and at a much faster rate than the motion of the larger droplets.

Movie S3 | The shape changes of a liquid Pb nanodroplet after the cap of the nanocontainer is punctured. The evaporation kinetics indicates a transition between pinned and moving contact line regimes.

Movie S4 | The phase transition of a large Pb particle in the closed nanocup system while increasing temperature.

Movie S5 | When the container is ruptured, the motion of the nanodroplet. The motion of liquid Pb nanodroplet nearly stopped, and after 0.03 seconds, this stationary liquid Pb droplet suddenly moved toward the end (sealing) of the nanocontainer.

References

1. Yokota, T., Howe, J. M., Jesser, W. A. & Murayama, M. Fractional Brownian motion of an Al nanosphere in liquid Al-Si alloy under electron-beam irradiation. *J. Appl. Phys.*, **95**, 5756-5761 (2004).
2. Hobbs, L. W. Introduction to analytical electron microscopy (Eds. J. J. Hren, J. I. Goldstein & D. C. Joy), Plenum Press, New York.
3. Williams, D. B. & Carter, C. B. Transmission Electron Microscopy (Plenum Press, New York, 1996).
4. Egerton, R. F., McLeod, R., Wang, F. & Malac, M. Basic questions related to electron-induced sputtering in the TEM. *Ultramicroscopy*, **110**, 991-997 (2010).
5. Ehrhart, P., Jung, P., Schultz, H. & Ullmaier, H. *Springer Materials, Landolt-Börnstein database, Group III: Crystal and Solid State Physics, Volume 25 Atomic Defects in Metals* (Springer-Verlag, 1991), p. 18.
6. Kudriavtsev, Y., Villegas, A., Godines, A. & Asomoza, R. Calculation of the surface binding energy for ion sputtered particles. *Appl. Sur. Sci.* **239**, 273-278 (2005).